Title

Energy decomposition analysis of single bonds within Kohn–Sham density functional theory

Journal

Proceedings of the National Academy of Sciences of the United States of America, 114(48)

ISSN

0027-8424

Authors

Levine, Daniel S

Head-Gordon, Martin

Publication Date

2017-11-28

DOI

10.1073/pnas.1715763114

Peer reviewed

Energy Decomposition Analysis of Single Bonds Within Kohn-Sham Density Functional Theory

Daniel S. Levine[a] **and Martin Head-Gordon**[a,*]

[a]Kenneth S. Pitzer Center for Theoretical Chemistry, Department of Chemistry, University of California, Berkeley, California 94720, USA and Chemical Sciences Division, Lawrence Berkeley National Laboratory Berkeley, California 94720, USA

This manuscript was compiled on October 3, 2017

An energy decomposition analysis (EDA) for single chemical bonds is presented within the framework of Kohn-Sham density functional theory, based on spin-projection equations that are exact within wavefunction theory. Chemical bond energies can then be understood in terms of stabilization due to spin-coupling, augmented by dispersion, polarization, and charge transfer in competition with destabilizing Pauli repulsions. The EDA reveals distinguishing features of chemical bonds ranging across non-polar, polar, ionic and charge-shift bonds. The effect of electron correlation is assessed by comparison with Hartree-Fock results. Substituent effects are illustrated by comparing the C-C bond in ethane against that in bis(diamantane), and dispersion stabilization in the latter is quantified. Finally, three metal–metal bonds in experimentally characterized compounds are examined: a $Mg^{I}-Mg^{I}$ dimer, the $Zn^{I}-Zn^{I}$ bond in dizincocene, and the Mn−Mn bond in dimanganese decacarbonyl.

Energy Decomposition Analysis | Chemical Bonding

Understanding the chemical bond is central to both synthetic and theoretical chemists. The approach of the synthetic chemists is based on qualitative, empirical features (electronegativity, polarizability, etc.) gleaned over the past 150 years of research and investigation. These features are notably absent from the toolbox of the theoretical chemist, who relies on a quantum mechanical wavefunction to holistically describe the electronic structure of a molecule; in essence, a numerical experiment. Bridging this gap is the purview of bonding analysis and energy decomposition analysis (EDA), which seeks to separate the quantum mechanical energy into physically meaningful terms. Bonding analysis and EDA approaches are necessarily non-unique, but different well-designed approaches provide complementary perspectives on the nature of the chemical bond. This task is not yet complete, despite intensive effort and substantial progress(1–5).

The chemical bond was originally viewed(6) as being electrostatic in origin, based on the virial theorem, and supported by an accumulation of electron density in the bonding region relative to superposition of free atom densities. The chemical bond is still often taught this way in introductory classes. However, the quantum mechanical origin of the chemical bond in H_2^+ and H_2 (classical mechanics does not explain bonding) lies in lowering the kinetic energy by delocalization, that is, via constructive wavefunction interference. This was first established(1) 55 years ago by Ruedenberg for H_2^+. A secondary effect, in some cases, such as in H_2, is orbital contraction, which is most easily seen by optimizing the form of a spherical 1s function as a function of bond-length(7). Polarization and charge-transfer contribute to further stabilization.

Analyzing chemical bonds in more complex molecules has also attracted great attention. Ruedenberg and co-workers have been developing generalizations of their classic analysis procedures with this objective(8, 9). Valence bond theory, while uncompetitive for routine computational purposes, involves conceptually simple wave functions that are suitable for extracting qualitative chemical bonding concepts(10). The emergence of the "charge-shift bond" paradigm, exemplified by the F_2 molecule, is a specific example of its value(11). The widely used Natural Bond Orbital (NBO) approach (12), provides localized orbitals, predominant Lewis structures, and information on hybridization and chemical bonds. The quantum theory of atoms-in-molecules (QTAIM) (13), describes the presence of bonds by so-called bond critical points in the electron density, as well as partitioning an energy into intra-atomic and inter-atomic terms. Another topological approach is the electron localization function (ELF), which is a function of the density and the kinetic energy density. Many other methods also exist for partitioning a bond energy into sums of terms that are physically interpretable (4).

EDA schemes have been very successful at elucidating the nature of non-covalent interactions(2, 14, 15). These methods typically separate the interaction energy by either perturbative approaches or constrained variational optimization. Perturbative methods include the popular Symmetry Adapted Perturbation Theory (SAPT)(16, 17) method and the Natural Energy Decomposition Analysis (NEDA)(18), based on NBOs. Variational methods include Kitaura and Morokuma (KM) EDA(19), the Ziegler-Rauk method(20), the Block-Localized Wavefunction (BLW-EDA)(14) and the Absolutely Localized Molecular Orbital (ALMO-EDA) of Head-Gordon et al(21–24). A number of non-covalent EDA methods have been applied to

Significance Statement

While theoretical chemists today can calculate the energies of molecules with high accuracy, the results are not readily interpretable by synthetic chemists who use a different language to understand and improve chemical syntheses. Energy decomposition analysis (EDA) provides a bridge between theoretical calculation and the practical insight. Most existing EDA methods are not designed for studying covalent bonds. We developed an EDA to characterize single bonds, providing an interpretable chemical fingerprint in the language of synthetic chemists from the quantum mechanical language of theorists.

MHG designed research; DSL performed research; Both analyzed data and wrote the paper.

The authors declare no conflicts of interest.

*To whom correspondence should be addressed. E-mail: mhg@cchem.berkeley.edu

bonds(2, 20, 25), although the single-determinant nature of these methods leads to spin-symmetry broken wavefunctions, which contaminates the EDA terms with effects from the other terms.

To address this challenge, we recently reported a spin-pure extension of the ALMO-EDA scheme to the variational analysis of single covalent bonds(26). The method, which reduces to the ALMO-EDA scheme for non-covalent interactions(24), includes modified versions of the usual non-bonded frozen orbital (FRZ), polarization (POL) and charge transfer (CT) terms, as well as a new spin-coupling (SC) term describing the energy lowering due to electron pairing. The final energy corresponds to the CAS(2,2) (equivalently, 1-pair perfect-pairing or TCSCF) wavefunction. While this is a fully ab initio model, it lacks the dynamic correlation necessary for reasonable accuracy.

By far the most widely used treatment of dynamic correlation in quantum chemistry today is Kohn-Sham density functional theory (DFT)(27). DFT methods yield RMS errors in chemical bond strengths on the order of a few kcal/mol, which approaches chemical accuracy at vastly lower computational effort than wavefunction methods. The purpose of this paper is to recast our bonded ALMO-EDA method into a single-determinant formalism that allows the computation of a dynamically-correlated bonded EDA with any existing density functional. After outlining our approach, we turn to the characterization of a variety of chemical bonds, ranging from familiar systems, to less familiar dispersion stabilized bonds, and several single metal-metal bonds.

Variational energy decomposition analysis

The single bond of interest is by definition the difference between the DFT calculation on the molecule, and the sum of DFT calculations on the separately optimized, isolated fragments. This interaction will be separated into five terms:

$$\begin{aligned}\Delta E_{\rm int} =& E_{\rm molecule} - \sum_{Z}^{\rm frags} E_Z \\ =& \Delta E_{\rm PREP} + \Delta E_{\rm FRZ} + \Delta E_{\rm SC} + \Delta E_{\rm POL} + \Delta E_{\rm CT} \quad [1]\end{aligned}$$

Each term is described in a corresponding subsection below.

Preparation energy. We begin from two doublet radical fragments, each of which is described by a restricted open shell (RO) HF or Kohn-Sham DFT single determinant whose orbitals are obtained in isolation from the other. $\Delta E_{\rm PREP}$ includes the energy required to distort each radical fragment to the geometry it adopts in the bonded state, $\Delta E_{\rm GEOM}$. This "geometric distortion" arises in most EDAs.

There is a further distortion energy that may also be incorporated into $\Delta E_{\rm PREP}$. Many radicals have a different hybridization than in the corresponding bond. For example, an F atom has an unpaired electron in a p-orbital while an F atom in a bond will be sp-hybridized. Or, the amine radical, NH_2, is sp^2-hybridized with an unpaired electron in a p-orbital, while an amine group is often sp^3-hybridized or sp^2-hybridized with a lone pair in the p-orbital in a molecule. Rearranging the odd electron of each radical fragment to be in the hybrid orbital that is appropriate for spin-coupling will incur an energy cost, $\Delta E_{\rm HYBRID}$, that completes the preparation energy:

$$\Delta E_{\rm PREP} = \Delta E_{\rm GEOM} + \Delta E_{\rm HYBRID} \quad [2]$$

We define $\Delta E_{\rm HYBRID}$ as the energy change due to rotations of the β hole in the span of the α occupied space from the isolated radical fragment to the correct arrangement in the bond. This is accomplished by variational optimization of the fragments' RO orbitals (in the spin-coupled state) only allowing doubly occupied-singly occupied mixings. Afterwards the modified fragment orbitals are used to evaluate $\Delta E_{\rm HYBRID}$. As limited orbital relaxation is involved, $\Delta E_{\rm HYBRID}$ may also be viewed as a kind of polarization and indeed it was previously placed in the POL term.(26)

However, $\Delta E_{\rm HYBRID}$ is also partially present here in that the geometry of the radical fragment is fixed to be that of the *interacting* fragment. For instance, free methyl radical is an sp^2-hybridized planar molecule while a methyl group in a bond is a pyramidalized sp^3 fragment, and it is the latter that is employed in this EDA scheme. We have moved $\Delta E_{\rm HYBRID}$ here for that reason, and because it can be much larger than the other contributions to POL and therefore its presence in POL can obscure trends in POL and SC across rows as the hybridization of the radical fragment changes.*

Nevertheless, regarding orbital rehybridization as part of preparation (as we do in this paper) or as part of polarization (as was done previously(26)) are both defensible choices. And in cases where $\Delta E_{\rm HYBRID}$ is large, the consequences of where it is placed can be considerable, as $\Delta E_{\rm PREP}$, $\Delta E_{\rm FRZ}$, $\Delta E_{\rm SC}$, and $\Delta E_{\rm POL}$ all change as a result. So the reader can compare, and decide whether they agree with our present choice, corresponding data tables with rehybridization as part of polarization (and $\Delta E_{\rm PREP} = \Delta E_{\rm GEOM}$) are included in the Supporting Information.

Frozen energy. The second term in Eq. (1), $\Delta E_{\rm FRZ}$, is the energy change associated with the two radical fragments interacting without permitting spin-coupling, polarization or charge-transfer. For simplicity (but without loss of generality) let us assume both radicals have $S = \frac{1}{2}; M_S = +\frac{1}{2}$. In the frozen (FRZ) energy, the fragment wavefunctions are combined to form a spin-pure triplet single determinant wavefunction ($S = 1; M_S = +1$) without allowing the orbitals to relax. This term is entirely a non-bonded interaction and will typically be repulsive for a chemical bond due to Pauli repulsion. It includes contributions from inter-fragment electrostatics, Pauli repulsion, exchange-correlation, and dispersion. The addition of dispersive effects, a dynamic correlation property, using DFT should result in smaller frozen energy terms than what is calculated in the original CAS(2,2) ALMO-EDA method.

A set of orbitals is said to be "absolutely localized" if the MO coefficient matrix is block-diagonal in the fragments. Since the atoms partition into fragments, so do their corresponding

*Even with $\Delta E_{\rm PREP}$ so defined, one must still reorient the frozen orbitals to resolve degeneracies and obtain the correctly oriented closed-shell density, as previously described(26).

AOs, and hence, the isolated fragment MOs, $\mathbf{T}$, automatically satisfy the ALMO constraint. The "frozen" occupied ALMOs constructed by block diagonally concatenating isolated restricted open-shell fragments need not be orthogonal (ALMOs are generally nonorthogonal) so they have an overlap matrix, σ. Therefore, as a function of interfragment separation, the frozen density matrix, $\mathbf{P}_{\mathrm{FRZ}} = \mathbf{T}\sigma^{-1}\mathbf{T}^{\dagger}$, undergoes Pauli deformation, even though $\mathbf{T}$ is constant.

The energy associated with this density (E_{FRZ}) may then be computed by HF or DFT. The frozen interaction energy is the difference relative to non-interacting, prepared fragments:

$$\Delta E_{\mathrm{FRZ}} = E_{\mathrm{FRZ}} - \sum_{Z}^{\mathrm{frags}} E_Z \qquad [3]$$

This ALMO-EDA FRZ term may be further separated into contributions corresponding to permanent electrostatic interactions, Pauli repulsion, and dispersion(23).

Spin-coupling. The third term in Eq. (1), ΔE_{SC}, is the energy difference due to electron pairing: that is, changing the spin coupling (SC) of the two radical electrons from high-spin triplet to low-spin singlet. The spin-coupling energy accounts for the difference between destructive wavefunction interference (in the high-spin case) and constructive wavefunction interference (in the low-spin case). It is worth pointing out that delocalization does not require two spins and is present even in $H_2{}^+$. Like FRZ, SC will be evaluated with frozen orbitals, but while FRZ is typically strongly repulsive (dominated by Pauli repulsion), SC is typically strongly attractive in the overlapping regime associated with covalent bond formation. For this reason, and because we are primarily interested in the singlet surface (as opposed to the triplet surface of the initial supersystem), FRZ and SC may be grouped together into a frozen orbitals term (FRZ+SC).

From the high-spin frozen determinant ($S = 1; M_S = +1$), flipping the spin ($\alpha \rightarrow \beta$) of one of the two half-occupied orbitals reduces the M_S value by one (i.e. $M_S = +1 \longrightarrow M_S = 0$). The objective is to change the spin coupling from (not bonding) triplet to (bonding) singlet. But in the single determinant formalism, the result of the spin-flip is a broken symmetry (BS) ALMO determinant. Its energy, E_{BS}, contains the desired spin-coupled low-spin (LS) energy, E_{LS}, but also a single *contaminant*, which is high spin (HS): $E_{\mathrm{HS}} = E_{\mathrm{FRZ}}$, and $S_{\mathrm{HS}} = S_{\mathrm{LS}} + 1$. We may write:

$$E_{\mathrm{BS}} = (1-c)E_{\mathrm{LS}} + cE_{\mathrm{HS}} \qquad [4]$$

To obtain c, we examine the value of $\langle S^2\rangle_{\mathrm{BS}}$ which is contaminated in exactly the same way as the energy:

$$\begin{aligned}\langle S^2\rangle_{\mathrm{BS}} &= (1-c)\langle S^2\rangle_{\mathrm{LS}} + c\langle S^2\rangle_{\mathrm{HS}} \\ &= \langle S_z\rangle_{\mathrm{LS}}(\langle S_z\rangle_{\mathrm{LS}} + 1) + 2c(\langle S_z\rangle_{\mathrm{LS}} + 1) \qquad [5]\end{aligned}$$

Using the calculated $\langle S^2\rangle_{\mathrm{BS}}$ value (a derivation of the $\langle S^2\rangle$ value for a broken symmetry single determinant with non-orthogonal orbitals is given in the Supporting Information), we solve for c via Eq. (5):

$$c = \frac{\langle S^2\rangle_{\mathrm{BS}} - \langle S_z\rangle_{\mathrm{LS}}(\langle S_z\rangle_{\mathrm{LS}} + 1)}{2(\langle S_z\rangle_{\mathrm{LS}} + 1)} \qquad [6]$$

In turn, this permits us to solve Eq. (4) for the spin-pure energy, $E_{\mathrm{LS}} = \alpha E_{\mathrm{BS}} + (1-\alpha)E_{\mathrm{HS}}$, where $\alpha = (1-c)^{-1}$. This result corresponds to Yamaguchi's spin-projection scheme(28, 29). Finally, with E_{LS} in hand, the spin-coupling term is given by

$$\Delta E_{\mathrm{SC}} = E_{\mathrm{LS}} - E_{\mathrm{FRZ}} \qquad [7]$$

where the orbitals are still the frozen fragment ones.

The above derivation is exact because a spin-pure E_{LS} is obtained if $\langle S^2\rangle_{\mathrm{BS}}$ and $\langle E\rangle_{\mathrm{BS}}$ are evaluated consistently from the same 1- and 2-particle density matrices (PDMs). An example is the case of HF wavefunctions. Unfortunately, this condition is not strictly satisfied for Kohn-Sham DFT, because the interacting 2PDM is not available,(30) and thus the value of $\langle S^2\rangle_{\mathrm{BS}}$ corresponding to $\langle E\rangle_{\mathrm{BS}}$ is not available. This dilemma arises because the fundamental theorems of DFT allow construction of the exact ground state energy without knowledge of the 2PDM. The best that can be straightforwardly accomplished is to employ the non-interacting 2PDM (i.e. from the Kohn-Sham determinant) to evaluate $\langle S^2\rangle_{\mathrm{BS}}$ in DFT. For any functional but HF, this choice leads to a small inconsistency in the final energy whose remedy is described in the subsection on charge transfer below.

Regarding comparison of this approach with other EDAs, this SC term is only *partly* contained in the frozen orbital term in EDA schemes such as the Ziegler-Rauk approach(20) used extensively for bonding analysis(2). Such EDAs form only one frozen supersystem on the low-spin surface, rather than separate FRZ and SC terms. The resulting low-spin frozen energy is exactly E_{BS} above. From the analysis above, due to spin contamination, $\Delta E_{\mathrm{FRZ(BS)}} > \Delta E_{\mathrm{FRZ}} + \Delta E_{\mathrm{SC}}$.

Polarization. The fourth term in Eq. (1), ΔE_{POL}, arises partly from the orbitals (with low spin coupling) relaxing due to the presence of the field of the other fragment. ΔE_{POL} is the term that includes contributions from polarization in the bond, but the ALMO constraint prevents charge-transfer contributions. To provide a well-defined basis set limit, fragment electric response functions (FERFs) are used as the ALMO virtual basis (22, 24). The FERFs are the subset of virtual orbitals that exactly describe the linear response of each fragment to an applied electric field. Following previous work(22, 24), the dipole and quadrupole (DQ) FERFs will be used to define the fragment virtual spaces for electrical polarization. For a hydrogen atom, the 3 dipole functions are p-like, and the 5 quadrupole functions are d-like.

In addition to electrical polarization, there is another contribution to polarization that we have discussed in detail elsewhere(31). The frozen orbitals may contract towards the nucleus to lower their energy *without any induced electrical moments*. This contraction effect was first identified by Ruedenberg(1) as part of his classic analysis of the one-electron chemical bond in $H_2{}^+$. We have shown(31) that orbital contraction can be accurately modeled by adding a so-called monopole (M) function to the FERF virtual space for each occupied orbital. On the H atom, the monopole FERF is a 2s type function.

The overall FERF basis is thus of MDQ type, and thus:

$$\Delta E_{\mathrm{POL}} = \Delta E_{\mathrm{POL}}^{\mathrm{CON}} + \Delta E_{\mathrm{POL}}^{\mathrm{ELE}} \quad [8]$$

where(31), $\Delta E_{\mathrm{POL}}^{\mathrm{CON}} = E_{\mathrm{ALMO/M}} - E_{\mathrm{FRZ}}$ and $\Delta E_{\mathrm{POL}}^{\mathrm{ELE}} = E_{\mathrm{ALMO/MDQ}} - E_{\mathrm{ALMO/M}}$. Our results showed that orbital contraction was very important in bonds to hydrogen but rather insignificant in bonds only involving heavier elements(31). This decreased energy lowering in heavy element bonds can be viewed as arising from diminished violation of the virial theorem upon spin-coupling with frozen orbitals, relative to bonds to hydrogen.

The additional mathematics necessary to implement polarization in conjunction with the approximate DFT spin-projection method is described in the Supporting Information.

Charge-transfer. The final term, ΔE_{CT}, contains charge-transfer (CT) contributions, allowing electrons to move between the fragments. It is the dominant term in ionic bonds, and an important part of charge-shift bonds (11). Mathematically, we will release the ALMO constraint and reoptimize the orbitals to obtain an unconstrained spin-projected energy. Implemented with HF determinants, this gives the CAS(2,2)/1-pair perfect pairing energy. With DFT, we obtain the approximately spin-projected DFT analog, $E_{\mathrm{SP-DFT}}$.

However, as already mentioned, in DFT, the $\langle S^2 \rangle$ value used in the optimization is only approximate. Moreover, the approximate exchange-correlation functional accounts for some amount of static correlation. Hence, $E_{\mathrm{SP-DFT}}$ obtained at this final step is generally lower than the DFT energy of a single determinant, E_{DFT}. Since DFT functionals are typically developed (or fitted) to produce accurate results only as a single determinant, this overcounting of correlation leads to molecules being slightly overbound (on the order of 1-15 kcal/mol). To address this issue, we simply rescale the terms calculated on the approximately spin-projected low-spin surface by a factor, c_R, such that $\Delta E_{\mathrm{SC}} \leftarrow c_R \Delta E_{\mathrm{SC}}$, $\Delta E_{\mathrm{POL}} \leftarrow c_R \Delta E_{\mathrm{POL}}$, and $\Delta E_{\mathrm{CT}} \leftarrow c_R \Delta E_{\mathrm{CT}}$. c_R is defined as:

$$c_R = (E_{\mathrm{DFT}} - E_{\mathrm{FRZ}})/(E_{\mathrm{SP-DFT}} - E_{\mathrm{FRZ}}) \quad [9]$$

so that the final interaction energy exactly satisfies Eq. (1). These c_R are tabulated in the Supporting Information.

For DFT, this rescaling scheme will be inadequate for analyzing bonds whenever a single DFT determinant is itself inadequate to describe the bond, such as in strongly diradicaloid molecules. In such cases, it may be preferable to use the approximately spin-projected result directly, as is quite often done in broken symmetry DFT calculations(32, 33). In contrast, no rescaling would be needed for MP2 or coupled-cluster theory because the spin-projection would be exact, and such methods could additionally describe strongly diradicaloid systems.

Especially for symmetrical systems, one may inquire about the nature of the CT term. The spin-coupling term includes some amount of ionic-like contribution due to the non-orthogonality of the orbitals. In the limiting cases, when the singly-occupied spaces do not overlap at all, the spin-coupled state is purely covalent, and when they overlap fully, for symmetrical systems, the HF result is obtained. The CT term then measures the fraction of ionic contribution that was unavailable to the fragments with the FERF and ALMO Hilbert space constraints.

Computational Details

A development version of Q-Chem 4.4 was used for all calculations (34). All calculations were performed using the ωB97M-V density functional(35) (a range-separated hybrid (RSH) meta generalized gradient approximation (GGA)) and the aug-cc-pVTZ basis(36) unless otherwise specified. Numerical tests suggest that ωB97M-V is amongst the most accurate available for chemical bond energies(35). For decomposition of the frozen term(23), the dispersion-free functional employed with ωB97M-V was Hartree-Fock (HF). Decomposition of the frozen term was carried out using unrestricted fragments forming an unrestricted supersystem. While the preparation energy, Eq. (2), has two components, we report only their sum here (see supplementary material for the breakdown). Likewise, since the contraction energy has been discussed elsewhere(31), here we report only the total polarization energy, as defined in Eq. (8). Finally, when HF is used, identical EDA results (apart from the reclassification of the hybridization energy) are obtained as with the previously described multi-determinant (CAS(2,2) or 1PP) method, which is hereafter referred to as HF-EDA(26).

Results and Discussion

Representative Bonds. We first verify the behavior of the terms of the EDA by investigating some representative bonds with the ωB97M-V functional: the C−C bond in ethane (a nonpolar covalent bond), the H−Cl bond in HCl (a polar covalent bond), the F−Si bond in SiF_4 (a polar bond with ionic character), the F−F bond in F_2 (a non-polar, charge-shift bond), and the Li−F bond in LiF (an ionic bond) (see Figure 1 and Table 1). The EDA gives a "fingerprint" for different classes of bonds: covalent and charge-shift bonds have relatively high spin-coupling energies, polar bonds have relatively high polarization energies, charge-shift and ionic bonds have relatively high charge-transfer energies. The EDA thus recovers classical bonding concepts from quantum mechanical methods.(5)

Table 1. EDA of representative bonds (in kcal/mol). Values in parenthesis are the percentage of the total stabilizing interaction energy.

	PREP	FRZ	SC	POL	CT	Sum
H_3C-CH_3	36.9	279.7	-344.6 (82.7)	-11.8 (2.8)	-60.1 (14.4)	-99.8
H−Cl	13.1	219.0	-253.7 (74.7)	-49.3 (14.5)	-36.7 (10.8)	-107.5
$F-SiF_3$	41.5	259.1	-227.3 (48.9)	-119.0 (25.6)	-118.8 (25.5)	-164.4
F−F	9.2	186.3	-124.1 (52.7)	-37.2 (15.8)	-74.3 (31.5)	-40.1
Li−F	0.0	30.5	2.7	-7.8 (4.5)	-164.6 (95.5)	-139.2

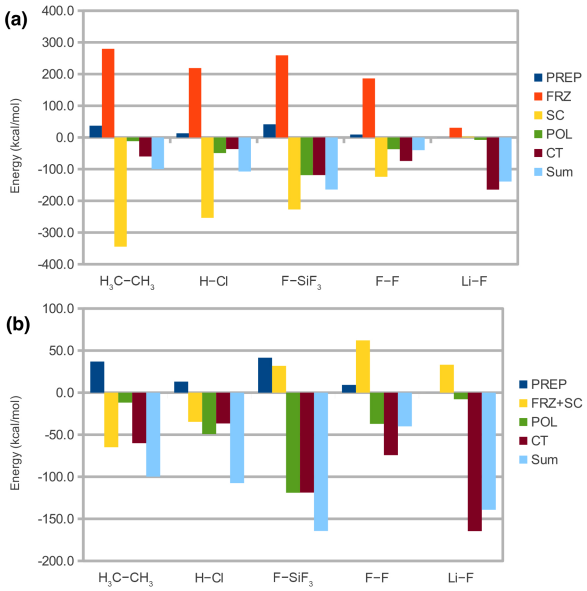

Fig. 1. a) EDA of representative single bonds. b) EDA of a few representative bonds with the FRZ and SC terms summed into a single frozen orbital term.

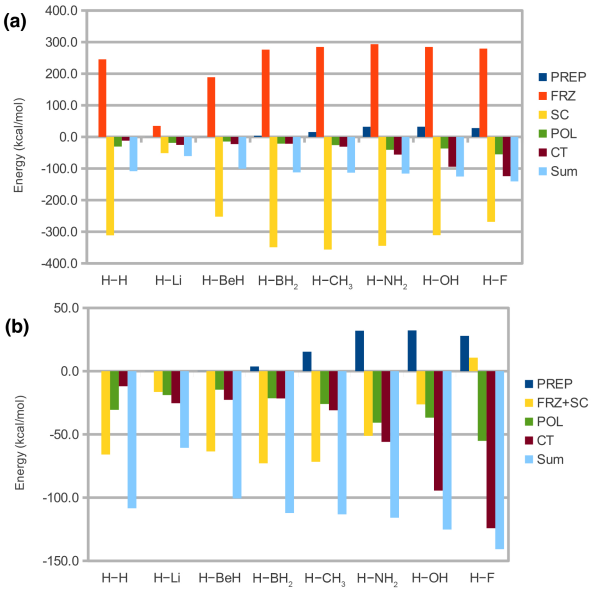

Fig. 2. a) EDA of first row element–H bonds. b) EDA of first row element–H bonds with the FRZ and SC terms summed into one frozen orbital term.

First-Row Element–H Bonds. This method allows us to investigate trends across periods and down groups of the periodic table. To illustrate, first-row element–H bonds were investigated (see Figure 2 and Table 2). Moving right across the first row, the elements become more electronegative and the E−H bonds switch from being non-polar covalent bonds to polar covalent bonds with increasing charge-transfer. This change is most obvious when the FRZ and SC terms are summed into a total frozen orbital term (Figure 2(b)). For the non-polar covalent bonds, total frozen orbital interactions (FRZ+SC) account for most of the bond energy. By contrast, in the moderately polar covalent bond in ammonia, POL becomes significant, and with increasing ionic character in water and HF, CT is a large source of binding.

Table 2. EDA of first-row E−H bonds (in kcal/mol). Numbers in parenthesis are the percentage of the total stabilizing interaction energy.

	PREP	FRZ	SC	POL	CT	Sum
H−H	0.0	245.4	-311.4 (88.0)	-30.6 (8.6)	-11.9 (3.4)	-108.4
H−Li	0.0	34.8	-51.2 (53.7)	-18.9 (19.8)	-25.3 (26.5)	-60.6
H−BeH	0.1	188.8	-252.3 (87.1)	-14.6 (5.1)	-22.7 (7.8)	-100.6
$H-BH_2$	3.7	276.1	-349.0 (89.0)	-21.4 (5.5)	-21.6 (5.5)	-112.2
$H-CH_3$	15.4	284.6	-356.3 (86.2)	-26.0 (6.3)	-30.9 (7.5)	-113.2
$H-NH_2$	32.0	293.3	-344.5 (78.1)	-40.8 (9.2)	-55.9 (12.7)	-115.9
H−OH	32.2	284.6	-310.9 (70.3)	-36.7 (8.3)	-94.5 (21.4)	-125.2
H−F	27.9	279.4	-268.7 (60.0)	-55.1 (12.3)	-124.2 (27.7)	-140.8

A variety of density functionals were investigated to determine how the HF-EDA terms are altered by the inclusion of dynamic correlation as well as to check that this method is not too sensitive to choice of functional. Full data tables comparing HF, BLYP-D3 (a dispersion-corrected GGA), PBE0-D3 (a dispersion-corrected hybrid GGA(37)), ωB97X-D (a dispersion-corrected RSH GGA(38)), B97M-V (a meta-GGA(39) with VV10 non-local correlation), and ωB97M-V (a RSH meta-GGA(35) with VV10) for all of the bonds described above are available in the Supporting Information. Generally speaking, addition of dynamic correlation decreases the frozen energy (owing to the inclusion of dispersion), and increases charge-transfer and polarization stabilization relative to Hartree-Fock. Figure 3 demonstrates these trends for the C−C bond in ethane and the F−F bond in fluorine. Some differences between functionals are inevitable, as none are exact. Overall the small discrepancies evident in Figure 3 and in the Supporting Information appear acceptable.

Bonding in Halogens. Dynamic correlation effects in bonds are most pronounced when the local electron density is high, such as in molecules with many lone-pairs near each other(40). Hence, dynamic correlation is necessary for studying bonds such as those in halogens (see Figure 4). Comparing the HF-EDA and ωB97M-V-EDA of the homoatomic halogens F_2, Cl_2, and Br_2, we see that dynamic correlation is indeed very important to obtain correct bond energies. Moreover, in these molecules, inclusion of dynamic correlation mostly increases the CT term, and so it is dynamic correlation associated with greater electron delocalization that contributes most strongly to the stability of bonds between halogen atoms, as might be expected from a charge-shift bond. Dispersion plays only a modest role (≈9 kcal/mol) in these molecules. This charge-shift bonding, in which ionic structure contribute significantly to the ground state, is manifest in the chemistry of halogens, for example, in the stabilization of charge-separated species

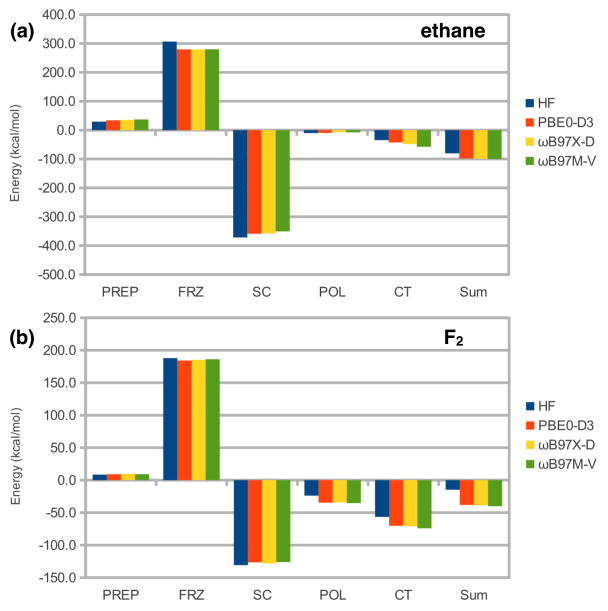

Fig. 3. Comparison of EDA terms computed at HF, PBE0-D3, ωB97X-D, ωB97M-V/aug-cc-pvtz of a) ethane and b) F_2

during the formation of halonium ions in the halogenation of alkenes.(41)

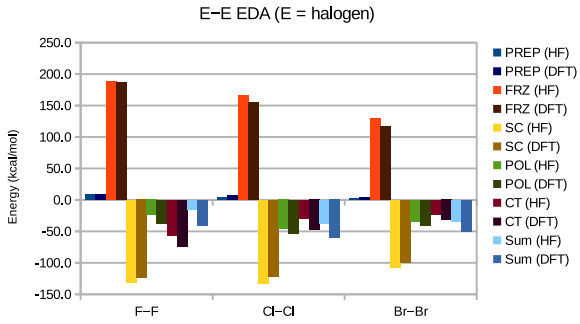

Fig. 4. Comparison of the EDA of the E−E bond (E = F, Cl, Br) computed at HF and ωB97M-V/aug-cc-pvtz (see also Table 3).

Dispersion-Assisted Bonds. In molecules with bulky side-groups, dispersion can play a significant role in the stabilization of bonds(42, 43). An example is the elongated 1.65 Å C−C bond in bis(diamantane), which, based on bond length is expected to have a bond strength of ≈40 kcal/mol(44). Experimentally, it is considerably stronger (showing no decomposition up to 300 °C), which has been attributed to many stabilizing dispersive interactions between the interfacial C−H bonds(45). Comparison of the EDA for this bond vs ethane (at the ωB97M-V/6-31+G** level) allows quantification of the forces that stabilize it, as shown in Table 4.

As seen in Table 4, while the POL and CT terms are fairly similar for ethane and bis(diamantane), the SC term is 82 kcal/mol less for bis(diamantane) following expectations based on bond length. However, the bis(diamantane) bond is not too much weaker than ethane because it also has a less destabilizing FRZ energy. Applying the ALMO frozen decomposition, it was found that dispersion accounts for this large increase in bond strength (60.4 kcal/mol vs. 8.3 kcal/mol of stabilization for bis(diamantane) and ethane, respectively). Enhanced dispersion is the key factor in accounting for the unusual stability of bis(diamantane), even as the bond-elongation is a result of partially relieving the close contacts.

Table 3. EDA of E−E bonds (E = halogen). All energies in kcal/mol. Numbers in parenthesis are the percentage of the total stabilizing interaction energy each term represents.

	PREP	FRZ	SC	POL	CT	Sum
F−F	9.2	186.3	-124.1 (52.7)	-37.2 (15.8)	-74.3 (31.5)	-40.1
Cl−Cl	6.8	154.8	-121.5 (54.7)	-52.8 (23.8)	-47.9 (21.6)	-60.6
Br−Br	4.4	116.4	-98.9 (57.7)	-40.7 (23.7)	-32.0 (18.6)	-50.8

Table 4. EDA of bis(diamantane) and ethane (ωB97M-V/6-31+G). All energies in kcal/mol. FRZ* is the frozen energy less the dispersion energy.**

	PREP	FRZ*	DISP	SC	POL	CT	Sum
diamantane	46.5	274.1	-60.4 (15.3)	-264.2 (66.8)	-23.1 (5.8)	-47.9 (12.1)	-75.1
H_3C-CH_3	37.6	285.9	-8.3 (2.0)	-346.5 (81.9)	-22.1 (5.2)	-46.4 (11.0)	-99.7

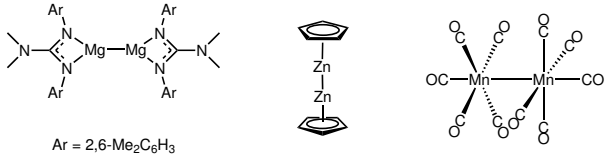

Fig. 5. Metal–metal bonds probed by the ALMO-EDA.

Metal–Metal Bonds. We next consider some single bonds which are less well studied: main-group and transition metal metal–metal bonds. We investigated a slightly truncated version of the Mg−Mg dimer of Jones and Stasch(46), the Zn−Zn bond in dizincocene from Carmona(47), and the classic Mn−Mn bond(48, 49) in the dimanganese decacarbonyl complex (see Figure 5). The relatively new Mg−Mg and Zn−Zn bonds are interesting for their novelty, and have proven to be important chemical synthons(50, 51). However, the nature of these symmetrically-bonded complexes is difficult to guess on first inspection because of our unfamiliarity with the chemistry of Mg and Zn in the formal +1 oxidation state. Will these be conventional covalent bonds, or will they have charge-shift character? These systems are therefore good candidates for use of the EDA, because we can compare their EDA results against the well-understood systems presented earlier.

The total bond energies obtained for the Mn−Mn bond is in close agreement with experimental measures (40.9 vs. 38 ± 5

kcal/mol) (52) and previous calculations(53, 54). There are no direct experimental measures for the given Mg−Mg and Zn−Zn bonds. The Mg−Mg bond in ClMgMgCl was extrapolated from experimental measurements to be 47.1 kcal/mol, in close agreement with the results obtained here.(55). Experimental Zn−Zn BDE measurements were obtained from the homoatomic dimer (which is, in principle, doubly-bonded), but the measured bond dissociation energy is relatively close to the Zn−Zn bond calculated here (82.2 vs. 93.7 kcal/mol).(56) Both classes of bonds have previously been studied by theoretical methods.(50, 57, and references therein)

The EDA results are given in Table 5. The Mg−Mg bond turn out to be a classic non-polar covalent bond analogous to H_2: the bond strength is mainly due to spin coupling (i.e. electron pairing) between the unpaired electrons on Mg(I) centers. There is almost no charge transfer: consistent with the high reduction potential of Mg(0), Mg(0)–Mg(II)/Mg(II)–Mg(0) contributions are not important in this bond. This is consistent with NBO calculations carried out in the initial disclosure of this molecule, which found the bond to be a covalent single-bond dominated by s-orbital contributions.(46)

On the other hand, the less reducing Zn in the Zn−Zn bond, which is principally covalent does exhibit some ionic Zn(0)–Zn(II)/Zn(II)–Zn(0) resonance contributions, much like in ethane. These ionic contributions account for most of why the Zn−Zn bond is stronger than the Mg−Mg bond. Our method provides an accurate dissection of the metal–metal bond in multimetallocenes, which was not possible before(58, 59). It also gives new insight into the origins of the relative bond strengths in metal–metal bonds: although both Mg−Mg and Zn−Zn bonds have strong covalent stabilization, the more easily oxidized Zn is further stabilized by ionic resonances, making it a much stronger bond. This was hinted at in a recent QTAIM study which showed that main-group–main-group bonds in M_2Cp_2 had more "covalent characteristics", while transition-metal–transition-metal bonds had "closed shell ionic characteristics".(60)

By contrast, the bond in dimanganese decacarbonyl is a charge-shift bond much like in F_2 with CT playing a major role in stabilizing the bond. Previous studies using QTAIM have also implicated "closed-shell interactions" and indicated that the bond is intermediate to a covalent and ionic bond (61) while other studies favor a more covalent picture(62). This hybrid covalent-CT stabilization is quantified here and appears analogous to the charge-shift bonding picture.(11)

Table 5. EDA of metal–metal bonds (ωB97X-D/6-31+G with BSSE correction). All energies in kcal/mol.**

	PREP	FRZ	SC	POL	CT	Sum
Mg−Mg	0.1	69.7	-118.3 (97.3)	-3.1 (2.5)	-0.2 (0.2)	-51.8
Zn−Zn	4.1	103.5	-150.0 (82.7)	-7.6 (4.2)	-23.7 (13.1)	-73.7
Mn−Mn	3.5	33.2	-37.4 (51.6)	-8.0 (11.1)	-27.0 (37.3)	-35.7

Comparison to Other EDA Methods. The main advantage of our EDA over alternatives for studying covalent bonds is its full use of valid, spin-pure intermediate wavefunctions. By contrast, the Morokuma EDA(19), Ziegler-Rauk EDA(2, 25) and the ETS-NOCV(20) method utilize broken-symmetry spin-contaminated intermediate wavefunctions to determine the energy components, which are likewise non-physically spin-contaminated.[†]. The degree of spin-contamination changes during the stepwise variational optimization of the wavefunction (e.g. the final state is typically a spin-pure and closed-shell), and hence the effect of the contamination is inconsistently distributed amongst the energy terms for a molecule. The spin-coupling energy of the method presented here is distributed between the Elec, Pauli, and Orb terms in a system-specific manner in these broken-symmetry based methods.

Another advantage of our EDA is that it can resolve different classes of chemical bonds. For comparison, the ZR-EDA/ETS-NOCV energy terms for H−H, H_3C-CH_3, F−F, and Li−F are given in Table 6. Note that no chemical fingerprint is evident from these data which significantly decreases the utility of broken-symmetry methods for understanding bonded interactions. It is unclear how much of the unphysical negative value of the H_2 Pauli repulsion is due to spin contamination versus self-interaction error of the functional. The ionic picture of LiF can be recovered with the Ziegler-Rauk method by first ionizing the fragments and noting a relatively small Orb term. However, this requires knowing how the fragments should be prepared, whereas in our method, the result falls out naturally.

Table 6. EDA of select bonds (ωB97M-V/aug-cc-pvtz) with broken-symmetry EDA methods. All energies in kcal/mol.

	H−H	H_3C-CH_3	F−F	Li−F	Li^+-F^-
Prep	0.0	17.9	0.0	0.0	45.6
Elec	3.9	-135.1	-41.9	-17.0	-202.2
Pauli	-10.9	194.1	165.2	55.1	42.9
Orb	-101.4	-175.5	-161.2	-176.1	-24.3

Conclusions

1. An energy decomposition analysis (EDA) method for single bonds has been developed in a single-determinant formalism. This EDA allows use of DFT with approximate spin-projection, thereby allowing for the efficient inclusion of dynamic correlation effects, such as dispersion.

2. Numerical tests show that the DFT-based EDA is not too sensitive to the choice of functional, and, relative to use of uncorrelated Hartree-Fock determinants, has improved the treatment of a variety of single bonds, including the first row E−H bonds and the bonds in halogens. Comparisons between different molecules should all be made with a single functional.

3. The inclusion of dispersion effects allows for meaningful study of bonds that rely heavily on dispersion, as illustrated by the example of bis(diamantane).

[†]This problem does not arise for intermolecular interactions, which are typically between closed shell fragments. In such cases, broken symmetry solutions do not enter and the ALMO-EDA frozen energy corresponds directly to that in these earlier EDAs.

4. Analysis of single metal–metal bonds with this method has permitted characterization of Mg(I)-Mg(I), Zn(I)-Zn(I), and Mn(0)-Mn(0) bonds that have been synthesized, and suggests physical reasons for the range of bond strengths seen in main group metal and transition metal bonds.

5. The main limitation of this EDA is its restriction to single chemical bonds. Only technical challenges inhibit the extension of this single bond EDA approach to correlated ab initio methods – we are currently working on addressing those issues.

Acknowledgements

This work was supported by grants (CHE-1665315 and CHE-1363342) from the U.S. National Science Foundation.

1. Ruedenberg K (1962) The Physical Nature of the Chemical Bond. *Rev. Mod. Phys.* 34(2):326–376.
2. Hopffgarten Mv, Frenking G (2012) Energy Decomposition Analysis. *WIREs Comput. Mol. Sci.* 2(1):43–62.
3. Frenking G, Shaik S, eds. (2014) *The Chemical Bond: Fundamental Aspects of Chemical Bonding.* (Wiley-VCH Verlag GmbH & Co. KGaA, Weinheim, Germany).
4. Rahm M, Hoffmann R (2015) Toward an Experimental Quantum Chemistry: Exploring a New Energy Partitioning. *J. Am. Chem. Soc.* 137(32):10282–10291.
5. Rahm M, Hoffmann R (2016) Distinguishing Bonds. *J. Am. Chem. Soc.* 138(11):3731–3744.
6. Slater JC (1933) The Virial and Molecular Structure. *J. Chem. Phys.* 1(10):687–691.
7. Bacskay GB, Nordholm S (2013) Covalent Bonding: The Fundamental Role of the Kinetic Energy. *J. Phys. Chem. A* 117(33):7946–7958.
8. Schmidt MW, Ivanic J, Ruedenberg K (2014) Covalent Bonds are Created by the Drive of Electron Waves to Lower their Kinetic Energy Through Expansion. *J. Chem. Phys.* 140(20):204104.
9. Cardozo TM, Nascimento MAC (2009) Energy partitioning for generalized product functions: The interference contribution to the energy of generalized valence bond and spin coupled wave functions. *J. Chem. Phys.* 130(10):104102.
10. Shaik S, Hiberty PC (2007) *A Chemist's Guide to Valence Bond Theory.* (John Wiley & Sons, Inc., Hoboken, NJ, USA).
11. Shaik S, Danovich D, Wu W, Hiberty PC (2009) Charge-shift bonding and its manifestations in chemistry. *Nat. Chem.* 1(6):443–449.
12. Reed AE, Curtiss LA, Weinhold F (1988) Intermolecular interactions from a natural bond orbital, donor-acceptor viewpoint. *Chem. Rev.* 88(6):899–926.
13. Bader RFW (1985) Atoms in molecules. *Acc. Chem. Res.* 18(1):9–15.
14. Mo Y, Bao P, Gao J (2011) Energy Decomposition Analysis Based on a Block-Localized Wavefunction and Multistate Density Functional Theory. *Phys. Chem. Chem. Phys.* 13(15):6760.
15. Phipps MJS, Fox T, Tautermann CS, Skylaris CK (2015) Energy Decomposition Analysis Approaches and their Evaluation on Prototypical Protein–Drug Interaction Patterns. *Chem. Soc. Rev.* 44(10):3177–3211.
16. Jeziorski B, Moszynski R, Szalewicz K (1994) Perturbation Theory Approach to Intermolecular Potential Energy Surfaces of van der Waals Complexes. *Chem. Rev.* 94(7):1887–1930.
17. Hohenstein EG, Sherrill CD (2012) Wavefunction methods for noncovalent interactions. *WIREs Comput. Mol. Sci.* 2(2):304–326.
18. Glendening ED (2005) Natural Energy Decomposition Analysis: Extension to Density Functional Methods and Analysis of Cooperative Effects in Water Clusters. *J. Phys. Chem. A* 109(51):11936–11940.
19. Kitaura K, Morokuma K (1976) A New Energy Decomposition Scheme for Molecular Interactions Within the Hartree-Fock Approximation. *Int. J. Quantum Chem.* 10(2):325–340.
20. Mitoraj MP, Michalak A, Ziegler T (2009) A Combined Charge and Energy Decomposition Scheme for Bond Analysis. *J. Chem. Theory Comput.* 5(4):962–975.
21. Khaliullin RZ, Cobar EA, Lochan RC, Bell AT, Head-Gordon M (2007) Unravelling the Origin of Intermolecular Interactions Using Absolutely Localized Molecular Orbitals. *J. Phys. Chem. A* 111(36):8753–8765.
22. Horn PR, Head-Gordon M (2015) Polarization Contributions to Intermolecular Interactions Revisited with Fragment Electric-Field Response Functions. *J. Chem. Phys.* 143(11):114111.
23. Horn PR, Mao Y, Head-Gordon M (2016) Defining the Contributions of Permanent Electrostatics, Pauli Repulsion, and Dispersion in Density Functional Theory Calculations of Intermolecular Interaction Energies. *J. Chem. Phys.* 144(11):114107.
24. Horn PR, Mao Y, Head-Gordon M (2016) Probing Non-Covalent Interactions with a Second Generation Energy Decomposition Analysis using Absolutely Localized Molecular Orbitals. *Phys. Chem. Chem. Phys.* 18(33):23067–23079.
25. Bickelhaupt FM, Baerends EJ (2000) Kohn-Sham Density Functional Theory: Predicting and Understanding Chemistry in *Reviews in Computational Chemistry*, eds. Lipkowitz KB, Boyd DB. (John Wiley & Sons, Inc.), pp. 1–86.
26. Levine DS, Horn PR, Mao Y, Head-Gordon M (2016) Variational Energy Decomposition Analysis of Chemical Bonding. 1. Spin-Pure Analysis of Single Bonds. *J. Chem. Theory Comput.* 12(10):4812–4820.
27. Klimeš J, Michaelides A (2012) Perspective: Advances and challenges in treating van der Waals dispersion forces in density functional theory. *J. Chem. Phys.* 137(12):120901.
28. Yamaguchi K, Jensen F, Dorigo A, Houk KN (1988) A spin correction procedure for unrestricted Hartree-Fock and Møller-Plesset wavefunctions for singlet diradicals and polyradicals. *Chem. Phys. Lett.* 149(5):537–542.
29. Kitagawa Y et al. (2007) Approximately spin-projected geometry optimization method and its application to di-chromium systems. *Chem. Phys. Lett.* 442(4–6):445–450.
30. Gilbert TL (1975) Hohenberg-Kohn theorem for nonlocal external potentials. *Phys. Rev. B* 12(6):2111–2120.
31. Levine DS, Head-Gordon M (2017) Quantifying the Role of Orbital Contraction in Chemical Bonding. *J. Phys. Chem. Lett.* 8(9):1967–1972.
32. Mouesca JM (2014) Density functional theory-broken symmetry (DFT-BS) methodology applied to electronic and magnetic properties of bioinorganic prosthetic groups. *Methods Mol. Biol.* 1122:269–296.
33. Ferré N, Guihéry N, Malrieu JP (2015) Spin decontamination of broken-symmetry density functional theory calculations: deeper insight and new formulations. *Phys. Chem. Chem. Phys.* 17(22):14375–14382.
34. Shao Y et al. (2015) Advances in molecular quantum chemistry contained in the Q-Chem 4 program package. *Mol. Phys.* 113(2):184–215.
35. Mardirossian N, Head-Gordon M (2016) omegaB97m-V: A combinatorially optimized, range-separated hybrid, meta-GGA density functional with VV10 nonlocal correlation. *J. Chem. Phys.* 144(21):214110.
36. Dunning TH (1989) Gaussian basis sets for use in correlated molecular calculations. I. The atoms boron through neon and hydrogen. *J. Chem. Phys.* 90(2):1007–1023.
37. Grimme S (2006) Semiempirical GGA-type density functional constructed with a long-range dispersion correction. *J. Comput. Chem.* 27(15):1787–1799.
38. Chai JD, Head-Gordon M (2008) Long-range corrected hybrid density functionals with damped atom–atom dispersion corrections. *Phys. Chem. Chem. Phys.* 10(44):6615–6620.
39. Mardirossian N, Head-Gordon M (2015) Mapping the genome of meta-generalized gradient approximation density functionals: The search for B97m-V. *J. Chem. Phys.* 142(7):074111.
40. Maksić ZB, ed. (1991) *Theoretical Models of Chemical Bonding.* (Springer Berlin Heidelberg, Berlin, Heidelberg).
41. McMurry JE (2015) *Organic Chemistry.* (Brooks Cole, Boston, MA, USA), 9 edition edition.
42. Wagner JP, Schreiner PR (2015) London Dispersion in Molecular Chemistry—Reconsidering Steric Effects. *Angew. Chem. Int. Ed.* 54(42):12274–12296.
43. Liptrot DJ, Guo JD, Nagase S, Power PP (2016) Dispersion Forces, Disproportionation, and Stable High-Valent Late Transition Metal Alkyls. *Angew. Chem. Int. Ed.* 55(47):14766–14769.
44. Zavitsas AA (2003) The Relation between Bond Lengths and Dissociation Energies of Carbon-Carbon Bonds. *J. Phys. Chem. A* 107(6):897–898.
45. Schreiner PR et al. (2011) Overcoming lability of extremely long alkane carbon-carbon bonds through dispersion forces. *Nature* 477(7364):308–311.
46. Green SP, Jones C, Stasch A (2007) Stable Magnesium(I) Compounds with Mg-Mg Bonds. *Science* 318(5857):1754–1757.
47. Resa I, Carmona E, Gutierrez-Puebla E, Monge A (2004) Decamethyldizincocene, a Stable Compound of Zn(I) with a Zn-Zn Bond. *Science* 305(5687):1136–1138.
48. Dahl LF, Rundle RE (1963) The crystal structure of dimanganese decacarbonyl Mn2(CO)10. *Acta Cryst.* 16(5):419–426.
49. Churchill MR, Amoh KN, Wasserman HJ (1981) Redetermination of the crystal structure of dimanganese decacarbonyl and determination of the crystal structure of dirhenium decacarbonyl. Revised values for the manganese-manganese and rhenium-rhenium bond lengths in dimanganese decacarbonyl and dirhenium decacarbonyl. *Inorg. Chem.* 20(5):1609–1611.
50. Jones C, Stasch A (2013) Stable Molecular Magnesium(I) Dimers: A Fundamentally Appealing Yet Synthetically Versatile Compound Class in *Alkaline-Earth Metal Compounds*, Topics in Organometallic Chemistry, ed. Harder S. (Springer Berlin Heidelberg) No. 45, pp. 73–101. DOI: 10.1007/978-3-642-36270-5_3.
51. Li T, Schulz S, Roesky PW (2012) Synthesis, reactivity and applications of zinc–zinc bonded complexes. *Chem. Soc. Rev.* 41(10):3759–3771.
52. Goodman JL, Peters KS, Vaida V (1986) The determination of the manganese-manganese bond strength in Mn2(CO)10 using pulsed time-resolved photoacoustic calorimetry. *Organometallics* 5(4):815–816.
53. Folga E, Ziegler T (1993) A density functional study on the strength of the metal bonds in Co2(CO)8 and Mn2(CO)10 and the metal-hydrogen and metal-carbon bonds in R-Mn(CO)5 and R-Co(CO)4. *J. Am. Chem. Soc.* 115(12):5169–5176.
54. Xie Y, Jang JH, King RB, Schaefer HF (2003) Binuclear Homoleptic Manganese Carbonyls: Mn2(CO)x (x = 10, 9, 8, 7). *Inorg. Chem.* 42(17):5219–5230.
55. Köppe R, Henke P, Schnöckel H (2008) MgCl and Mg2cl2: From Theoretical and Thermodynamic Considerations to Spectroscopy and Chemistry of Species with Mg-Mg Bonds. *Angew. Chem. Int. Ed.* 47(45):8740–8744.
56. Czajkowski MA, Koperski J (1999) The Cd2 and Zn2 van der Waals dimers revisited. Correction for some molecular potential parameters. *Spectrochim. Acta Mol. Biomol. Spectrosc.* 55(11):2221–2229.
57. Zhu Z et al. (2006) A Zinc–Zinc-Bonded Compound and Its Derivatives Bridged by One or Two Hydrogen Atoms: A New Type of Zn-Zn Bonding. *Angew. Chem. Int. Ed.* 45(35):5807–5810.
58. Velazquez A, Fernández I, Frenking G, Merino G (2007) Multimetallocenes. A Theoretical Study. *Organometallics* 26(19):4731–4736.
59. Pandey KK (2007) Energy analysis of metal-metal bonding in [RM-MR] (M = Zn, Cd, Hg; R = CH3, SiH3, GeH3, C5h5, C5me5). *J. Organomet. Chem.* 692(5):1058–1063.
60. Li X et al. (2013) Metal-Metal and Metal-Ligand Bonds in (eta5-C5h5)2m2 (M = Be, Mg, Ca, Ni, Cu, Zn). *Organometallics* 32(4):1060–1066.
61. Bianchi R, Gervasio G, Marabello D (2000) Experimental Electron Density Analysis of Mn2(CO)10: Metal-Metal and Metal-Ligand Bond Characterization. *Inorg. Chem.* 39(11):2360–2366.
62. Farrugia LJ, Mallinson PR, Stewart B (2003) Experimental charge density in the transition metal complex Mn2(CO)10: a comparative study. *Acta Crystallogr. Sect. B* 59(2):234–247.